SCATTERING OF PLANE SH-WAVE FROM A PARTIALLY DEBONDED SHALLOW CYLINDRICAL ELASTIC INCLUSION

J. X. Zhao [*] **H. Qi** [**]

College of Aerospace and Civil Engineering
Harbin Engineering University
Harbin, 150001, China

ABSTRACT

The scattering of plane SH-wave from a partially debonded shallow cylindrical elastic inclusion in half space is investigated in this paper by complex function method and expansion method of wave function. The debonding regions are considered as multiple arc-shaped interface cracks with non-contacting faces. Firstly, in the inclusion district, the standing wave function in the elastic inclusion with unknown coefficients which satisfies the boundary condition is constructed and generated into the Fourier series; in the half space, the stress and displacement boundary condition around the elastic inclusion can be modeled as the same as the standing wave function in the elastic inclusion. Then, a set of infinite algebraic equations can be obtained around the same boundary and the solution of problem can be gained. In the end, numerical examples of the surface displacement are provided and discussed. It is found that the interface cracks can raise the surface displacement amplitudes to a certain degree.

Keywords : Scattering of plane SH-wave, Multiple interface cracks, Complex function method, The surface displacement, Half space.

1. INTRODUCTION

The problem of the scattering and diffraction of plane SH-wave by the underground structures has been attracted much research attention. In the two-dimensional medium, the earlier reference to the analytic solution of the scattering of plane SH-wave by an underground inclusion existed in the article concerning an underground circular tunnel [1]. The analysis for cavities in the infinite space [2] and a cavity in a half space [3] were investigated. Other analytic solutions have been developed and applied to cavities of circular shape [4-6]. Dravinski [7] applied a boundary integral approach for irregularly shaped inclusions based on Green's functions. Using the weighted residual method, M. E. Manoogian [8] approached the scattering of plane SH-wave by an underground elastic inclusion of arbitrary shape in half-space. Lee [9] studied the three-dimensional spherical cavity in half-space. Recently, Chen [10,11] investigated the scattering of waves in a semi-analytical method.

However, it is noted that partial debonding may occur at the interface due to the low adhesion strength. So, in recent years, many scholars mostly focused on the dynamic analysis of the debonded inclusions. The wave scattering problems of a partially debonded circular cylinder were researched by Coussy [12,13], Belyaev [14], Yang and Norris [15-17] and Wang [18-20], including the cases of a circular liner partially debonded from a cavity [21] and a semi-cylindrical foundation embedded in a half-space [22]. Coussy [23] firstly studied the scattering of plane SH-wave by a partially debonded rigid elliptic inclusion using the conformal map technique and perturbation method and gave the far-field solution for the long-wavelength limit. In reference [24], the problem of an elliptic crack subjected to SH-wave was solved by using wave function expansion method in conjunction with singular integral equation technique, and then with this method, the case of an elastic and rigid elliptic inclusion with material constants slightly different to those of the matrix [25]. But few literatures have been found concerning debonded inclusions which perfectly buried in half space.

In this paper, the scattering of plane SH-wave from a debonded cylindrical elastic inclusion in half space is investigated. Some examples of the surface displacement are given and the influences by the inclusion, the incident wave and the debonding regions are discussed.

2. THE ANALYTIC MODEL

The local model to be studied is shown in the Fig. 1, which presents a partially debonded cylindrical elastic inclusion in half space impacted by the SH-wave with the angle α_0. The distance from the inclusion center to the horizontal interface is marked as h. Several debonding regions exists around the interface of the

[*] Ph.D., corresponding author [**] Professor

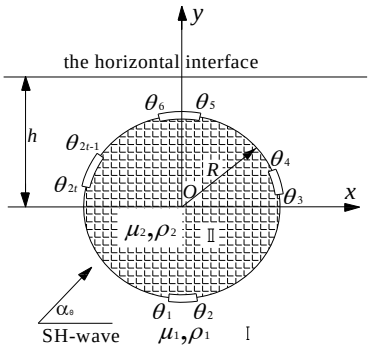

Fig. 1 The model of a partially debonded cylindrical elastic inclusion in half space

inclusion. Regarding the debonding parts as the non-contacting cracks, the cracks can be numbered from 1 to *t*. Accordingly, the starting and the end point can be noted θ_{2t-1}, θ_{2t} separately, in which, *t* is the number of the debonding region. In this subject, the whole district is divided into two parts. Figure 2 presents for the partially debonded cylindrical elastic inclusion, just medium II, with the shear modulus of elasticity, μ_2, the mass density ρ_2. Figure 3 shows a circular hole in half space, noted as medium I, the shear modulus of elasticity and the mass density can be written as μ_1, ρ_1.

3. FUNDAMENTAL THEORIES

3.1 Motion Equations

The dependence of displacement function *W* on time is $e^{-i\omega t}$ and *W* satisfies the following governing equation:

$$\frac{\partial^2 W}{\partial x^2}+\frac{\partial^2 W}{\partial y^2}+k^2 W=0 \tag{1}$$

where $k=\omega/c_s$, $c_s=\sqrt{\mu/\rho}$, ω is the circular frequency of displacement $W(x, y, t)$ and c_s stands for the shear wave velocity, and ρ, μ are the mass density and the shear modulus of elasticity respectively. The corresponding stresses are displayed as:

$$\tau_{xz}=\mu\frac{\partial W}{\partial x},\quad \tau_{yz}=\mu\frac{\partial W}{\partial y} \tag{2}$$

Used by the complex variables $z=x+iy$, $\bar{z}=x-iy$, Eqs. (1) and (2) can be expressed in the complex plain $(z,\bar{z})$ as :

$$\frac{\partial^2 W}{\partial z\,\partial \bar{z}}+\frac{1}{4}k^2 W=0 \tag{3}$$

$$\tau_{xz}=\mu\left(\frac{\partial W}{\partial z}+\frac{\partial W}{\partial \bar{z}}\right),\quad \tau_{yz}=i\mu\left(\frac{\partial W}{\partial z}-\frac{\partial W}{\partial \bar{z}}\right) \tag{4}$$

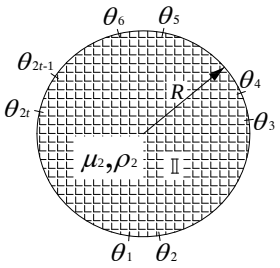

Fig. 2 The cylindrical elastic inclusion region

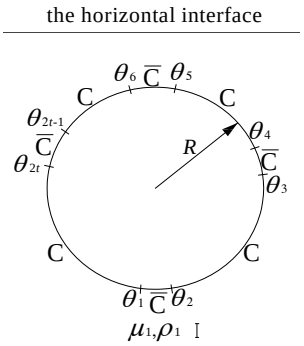

Fig. 3 The circular cavity in half space

The stress expressions in Eq. (4) can also be written in polar coordinate system as:

$$\begin{aligned}\tau_{rz}&=\mu\left(\frac{\partial W}{\partial z}e^{i\theta}+\frac{\partial W}{\partial \bar{z}}e^{-i\theta}\right)\\ \tau_{\theta z}&=i\mu\left(\frac{\partial W}{\partial z}e^{i\theta}-\frac{\partial W}{\partial \bar{z}}e^{-i\theta}\right)\end{aligned} \tag{5}$$

3.2 Subordinate Problems

According to reference [26], Figs. 2 and 3, in district II, standing wave function is constructed which satisfies the condition of stress free on the debonding regions, stress and displacement continuous with medium on the bonded region. We take it as:

$$\tau_{rz}^{(st)}=\begin{cases}0, & z\in\bar{C}\\ \dfrac{\mu_2 k_2 W_0}{2}\displaystyle\sum_{m=-\infty}^{\infty}C_m[J_{m-1}(k_2\,|\,z\,|) & \\ -J_{m+1}(k_2\,|\,z\,|)]\left[\dfrac{z}{|\,z\,|}\right]^m, & z\in C\end{cases} \tag{6}$$

In which, C_m are unknown coefficients, W_0 delegates the maximum value of the standing wave, which is given as 1.0 in this paper.

In general, the standing wave can be written as:

$$W^{(st)}=W_0\sum_{n=-\infty}^{\infty}D_n\,J_n\left(k_2\,|\,z\,|\right)\left[\frac{z}{|\,z\,|}\right]^n \tag{7}$$

Wherein, D_n are unknown coefficients.

Then, we can generate the Eq. (6) into the Fourier series in $[-\pi, \pi]$:

$$\tau_{rz}^{(st)} = \frac{\mu_2 k_2 W_0}{2} \sum_{n=-\infty}^{\infty} \sum_{m=-\infty}^{\infty} C_m a_{mn} \left[J_{m-1}(k_2 |z|) - J_{m+1}(k_2 |z|) \right] \cdot \left[\frac{z}{|z|} \right]^n \tag{8}$$

In which,

$$a_{mn} = \begin{cases} \dfrac{1}{2\pi} \left\{ 2\pi + \sum_{j=1}^{t} (\theta_{2j-1} - \theta_{2j}) \right\}, & m = n \\ \dfrac{\sum_{j=1}^{t} (e^{i(m-n)\theta_{2j-1}} - e^{i(m-n)\theta_{2j}})}{2\pi i (m-n)}, & m \neq n \end{cases} \tag{9}$$

Compared with the Eqs. (7) and (8), the related coefficients can be expressed as:

$$D_n = \sum_{m=-\infty}^{\infty} C_m \frac{J_{m-1}(k_2 R) - J_{m+1}(k_2 R)}{J_{n-1}(k_2 R) - J_{n+1}(k_2 R)} \; a_{mn} \tag{10}$$

According to the Eq. (8), the standing wave and the stress fields:

$$W^{(st)} = W_0 \sum_{n=-\infty}^{\infty} \sum_{m=-\infty}^{\infty} C_m \frac{J_{m-1}(k_2 R) - J_{m+1}(k_2 R)}{J_{n-1}(k_2 R) - J_{n+1}(k_2 R)} a_{mn} J_n(k_2 |z|) \left[\frac{z}{|z|} \right]^n \tag{11}$$

$$\tau_{rz}^{(st)} = \frac{\mu_2 k_2 W_0}{2} \sum_{n=-\infty}^{\infty} \sum_{m=-\infty}^{\infty} C_m \frac{J_{m-1}(k_2 R) - J_{m+1}(k_2 R)}{J_{n-1}(k_2 R) - J_{n+1}(k_2 R)} a_{mn} \left[J_{n-1}(k_2 |z|) - J_{n+1}(k_2 |z|) \right] \left[\frac{z}{|z|} \right]^n \tag{12}$$

$$\tau_{\theta z}^{(st)} = \frac{\mu_2 W_0 i}{|z|} \sum_{n=-\infty}^{\infty} \sum_{m=-\infty}^{\infty} n C_m \frac{J_{m-1}(k_2 R) - J_{m+1}(k_2 R)}{J_{n-1}(k_2 R) - J_{n+1}(k_2 R)} a_{mn} J_n(k_2 |z|) \left[\frac{z}{|z|} \right]^n \tag{13}$$

In district I, shown as Fig. 2, the scattering wave excited by the circular cavity $W^{(s)}$ can be constructed by the symmetry of the scattering wave, the related displacement field and stress field $\tau_{rz}^{(s)}$, $\tau_{\theta z}^{(s)}$ can be written as [27]:

$$W^{(s)} = \sum_{m=0}^{\infty} A_m \left\{ H_m^{(1)}(k_1 |z|) \cdot \left[\frac{z}{|z|} \right]^m + H_m^{(1)}(k_1 |z-2hi|) \cdot \left[\frac{z-2hi}{|z-2hi|} \right]^{-m} \right\} \tag{14}$$

$$\tau_{rz}^{(s)} = \frac{\mu_1 k_1}{2} \sum_{m=0}^{\infty} A_m \left\{ H_{m-1}^{(1)}(k_1 |z|) \cdot \left[\frac{z}{|z|} \right]^{m-1} \cdot e^{i\theta} - H_{m+1}^{(1)}(k_1 |z|) \cdot \left[\frac{z}{|z|} \right]^{m+1} \cdot e^{-i\theta} - H_{m+1}^{(1)}(k_1 |z-2hi|) \cdot \left[\frac{z-2hi}{|z-2hi|} \right]^{-(m+1)} \cdot e^{i\theta} + H_{m-1}^{(1)}(k_1 |z-2hi|) \cdot \left[\frac{z-2hi}{|z-2hi|} \right]^{-(m-1)} \cdot e^{-i\theta} \right\} \tag{15}$$

$$\tau_{\theta z}^{(s)} = \frac{i\mu_1 k_1}{2} \sum_{m=0}^{\infty} A_m \left\{ H_{m-1}^{(1)}(k_1 |z|) \cdot \left[\frac{z}{|z|} \right]^{m-1} \cdot e^{i\theta} + H_{m+1}^{(1)}(k_1 |z|) \cdot \left[\frac{z}{|z|} \right]^{m+1} \cdot e^{-i\theta} - H_{m+1}^{(1)}(k_1 |z-2hi|) \cdot \left[\frac{z-2hi}{|z-2hi|} \right]^{-(m+1)} \cdot e^{i\theta} - H_{m-1}^{(1)}(k_1 |z-2hi|) \cdot \left[\frac{z-2hi}{|z-2hi|} \right]^{-(m-1)} \cdot e^{-i\theta} \right\} \tag{16}$$

In which, A_m are unknown coefficients, which can be determined by the boundary condition.

4. SOLUTION OF PROBLEM

In a complete elastic half space, the incident steady plane SH-wave $W^{(i)}$ would be reflected from the interface. Both angle of incidence and reflection have the same value α_0, as shown in Fig. 1. In the complex plane, $W^{(i)}$ and $W^{(r)}$ can be given by:

$$W^{(i)} = W_0 \exp\left\{ \frac{ik}{2} \left[(z - ih) e^{-i\alpha_0} + (\bar{z} + ih) e^{i\alpha_0} \right] \right\} \tag{17}$$

$$W^{(r)} = W_0 \exp\left\{ \frac{ik}{2} \left[(z - ih) e^{i\alpha_0} + (\bar{z} + ih) e^{-i\alpha_0} \right] \right\} \tag{18}$$

The scattering wave $W^{(s)}$ has been obtained in Eq. (14).

Then, the total wave field in domain I is:

$$W = W^{(i)} + W^{(r)} + W^{(s)} \tag{19}$$

The corresponding stress can be written as:

$$\tau_{rz} = \tau_{rz}^{(i)} + \tau_{rz}^{(r)} + \tau_{rz}^{(s)}, \quad \tau_{\theta z} = \tau_{\theta z}^{(i)} + \tau_{\theta z}^{(r)} + \tau_{\theta z}^{(s)} \tag{20}$$

On the "C" boundary (Fig. 3), we have:

$$W^{(i)} + W^{(r)} + W^{(s)} = W^{(st)} \tag{21}$$

$$\tau_{rz}^{(i)} + \tau_{rz}^{(r)} + \tau_{rz}^{(s)} = \tau_{rz}^{(st)} \tag{22}$$

On the "$\overline{C}$" boundary (Fig. 3), we have:

$$\tau_{rz}^{(i)} + \tau_{rz}^{(r)} + \tau_{rz}^{(s)} = 0 = \tau_{rz}^{(st)} \tag{23}$$

From Eqs. (21) and (23), we can summary that on the whole boundary ("C" and $\overline{C}$):

$$\tau_{rz}^{(i)} + \tau_{rz}^{(r)} + \tau_{rz}^{(s)} = \tau_{rz}^{(st)} \tag{24}$$

In which, the independent variable θ ranges from $-\pi$ to π.

According to the solution of reference [26], the unknown coefficients A_m and C_m can be determined by the Eqs. (21) and (24).

5. THE SURFACE DISPLACEMENT AMPLITUDES

Impacted by incident steady-state plane SH-wave, it is significant to study the surface displacement in the geology and the underground engineering. Effected by the incident SH-wave, the whole wave field in the half space can be expressed as:

$$W^{(t)} = W^{(i)} + W^{(r)} + W^{(s)} \tag{25}$$

The nondimensional frequency η can be defined as:

$$\eta = 2R/\lambda = k_1 R/\pi \tag{26}$$

In which, λ is the length of wave, R is the characteristic dimension of the elastic inclusion. For the circular elastic inclusion, R is the radius of the circular inclusion. Additionally, η is a dimensionless number.

6. NUMERICAL EXAMPLES AND DISCUSSIONS

In this section, numerical examples for the surface displacement amplitudes are provided to show the disciplines of this subject. In the practical engineering, two kinds of familiar inclusions are the steel inclusion in granite medium and the concrete inclusion in granite medium. They present for two models of different characteristics.

Figure 4 shows the displacement amplitudes plotted on the horizontal interface above an elastic inclusion without any debonding region. The displacements are provided with the changes of the dimensionless x/a. The relate parameters are $\mu_2/\mu_1 = 1.0/6.0$, $\eta = 2.0$, $\rho_2/\rho_1 = 2.0/3.0$, $h/R = 1.5$. Figure 5 represents for the surface displacement on the ground above an elastic inclusion used by the weighted residual method [8]. The numerical results obtained in this paper (in Fig. 4) are consistent with the reference [8].

Figure 6 expresses the displacement amplitudes on the horizontal ground above a circular cavity with the parameters $h/R = 1.1$, $\eta = 1.25$, $\mu_2/\mu_1 = 0.0$, $\rho_2/\rho_1 = 1.0$. Figure 7 stands for the surface displacement on the ground above a circular cavity [27]. The results in Fig. 6 are also close to the outcome of reference [27] in Fig. 7.

In order to describe the effects by the debonding region, it is necessary to display the surface displacement amplitudes at two situations: With debonding region and without it.

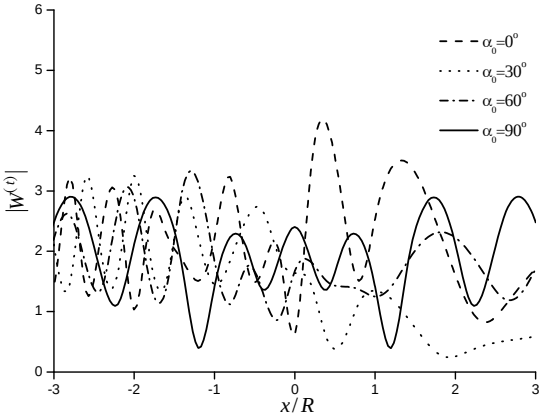

Fig. 4 The surface displacement amplitudes on the horizontal interface above a circular inclusion: $h/R = 1.5$, $\mu_2/\mu_1 = 1.0/6.0$, $\rho_2/\rho_1 = 2.0/3.0$, $\eta = 2.0$

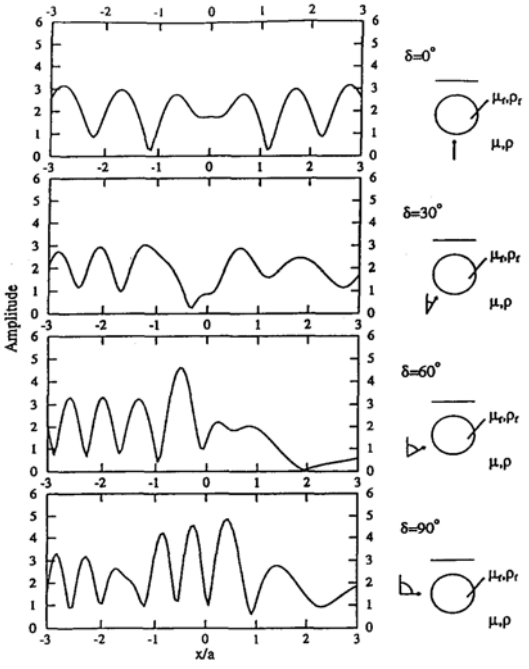

Fig. 5 The surface displacement amplitudes provided in reference [8] with the same parameters as Fig. 4

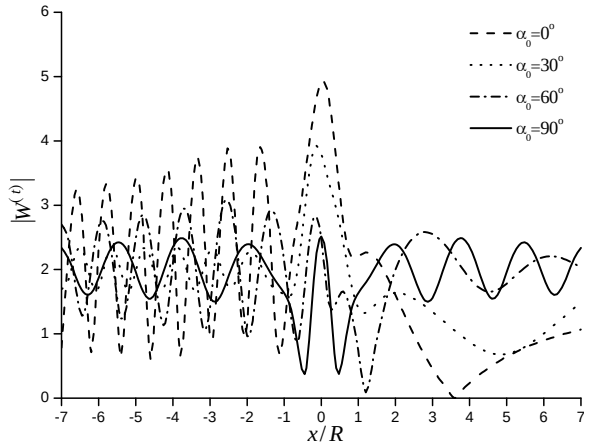

Fig. 6 The surface displacement amplitudes on the horizontal interface above a circular cavity: $h/R = 1.1$, $\mu_2/\mu_1 = 0.0$, $\rho_2/\rho_1 = 1.0$, $\eta = 1.25$

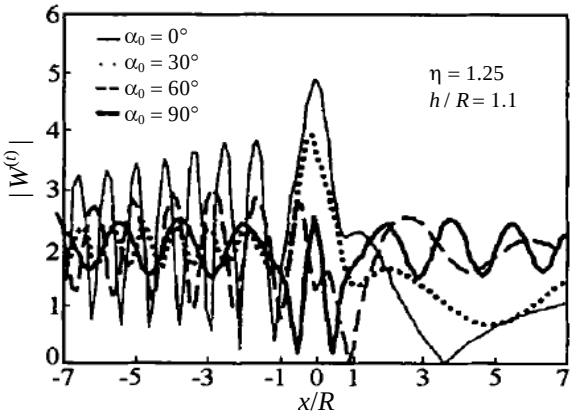

Fig. 7 The surface displacement amplitudes provided in reference [27] with the same parameters as Fig. 6

From Figs. 8 to 15, the ground surface displacements with a steel inclusion impacted by SH-wave are demonstrated. As shown in Figs. 16 to 19, the surface displacements with a concrete inclusion scattered by SH-wave are shown.

In which, the Figs. 8 to 11 represent the surface displacements in the low frequency ($\eta = 0.25$) with different angle α_0 of incident SH-wave. The angles of the debonding region are: $\theta_1 = 0°$, $\theta_2 = 30°$, $\theta_3 = 150°$, $\theta_4 = 180°$. From the numerical results, it is seen that the debonding region has slight influence to the surface ground in the low frequency compared with the situation without the debonding region. The incident angle effects largely on the surface displacement. For example, with $\alpha_0 = 0°$, the surface displacement amplitude can get 3.0, which is larger than the result with $\alpha_0 = 90°$.

As the increasing of α_0, the surface displacement effected by the SH-wave changes to some extent. When the SH-wave attacks vertically, the value of displacement changes in a small range around 2.0, which has slight effects on the surface ground. The essential reason for this phenomenon is the energy distribution of the SH-wave. With low α_0, the wave energy could

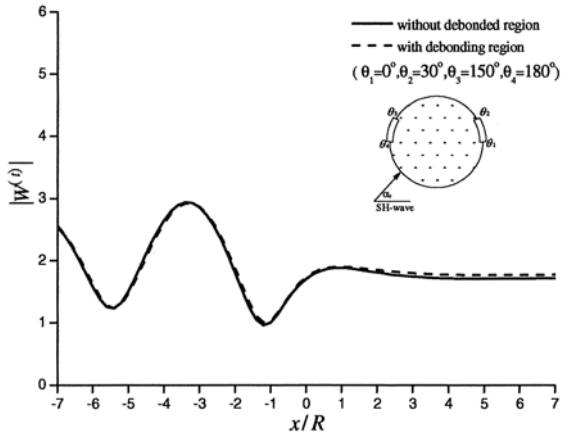

Fig. 8 The surface displacement amplitudes on the horizontal interface above an inclusion: $h/R = 1.5$, $\mu_2/\mu_1 = 3.23$, $\rho_2/\rho_1 = 1.52$, $\eta = 0.25$, $\alpha_0 = 0°$

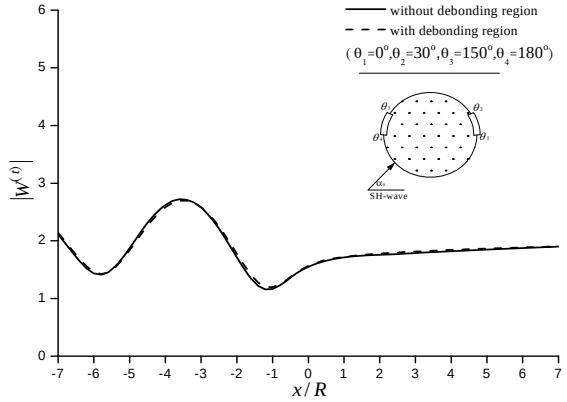

Fig. 9 The surface displacement amplitudes on the horizontal interface above an inclusion: $h/R = 1.5$, $\mu_2/\mu_1 = 3.23$, $\rho_2/\rho_1 = 1.52$, $\eta = 0.25$, $\alpha_0 = 30°$

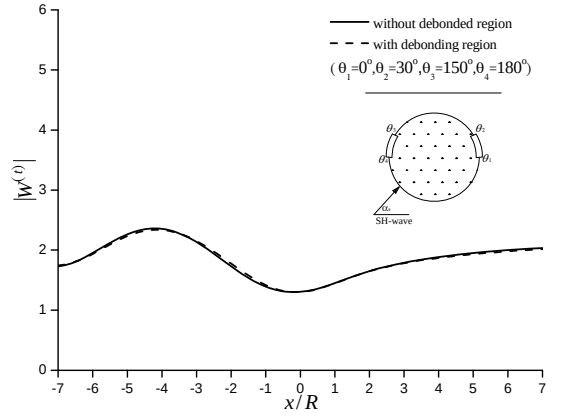

Fig. 10 The surface displacement amplitudes on the horizontal interface above an inclusion: $h/R = 1.5$, $\mu_2/\mu_1 = 3.23$, $\rho_2/\rho_1 = 1.52$, $\eta = 0.25$, $\alpha_0 = 60°$

assemble in the region of $x/a < 0.0$, due to the action of surface and the inclusion, the accumulated energy may act on the surface and enlarge the nearby displacement. So, the displacement in this region ($x/a < 0.0$), the displacement could even reach 3.0. On the account of the

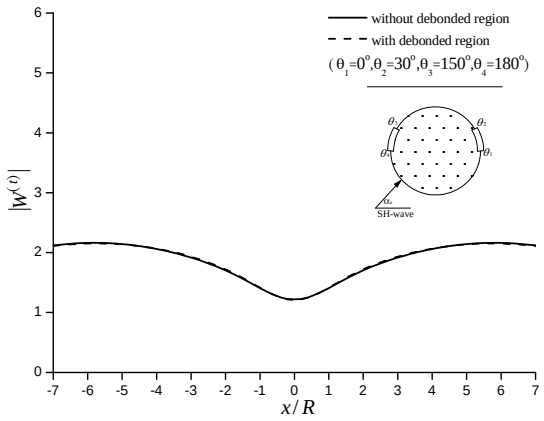

Fig. 11 The surface displacement amplitudes on the horizontal interface above an inclusion: $h/R = 1.5$, $\mu_2/\mu_1 = 3.23$, $\rho_2/\rho_1 = 1.52$, $\eta = 0.25$, $\alpha_0 = 90°$

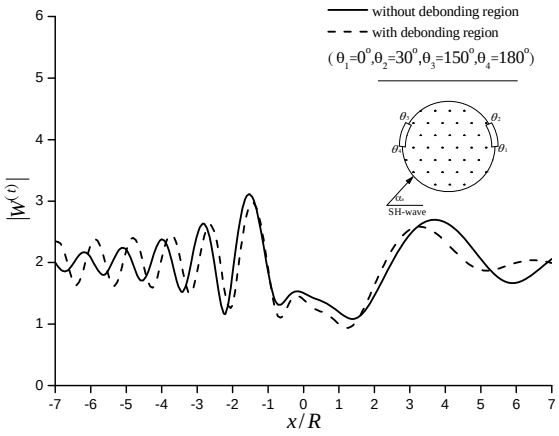

Fig. 14 The surface displacement amplitudes on the horizontal interface above an inclusion: $h/R = 1.5$, $\mu_2/\mu_1 = 3.23$, $\rho_2/\rho_1 = 1.52$, $\eta = 1.25$, $\alpha_0 = 60°$

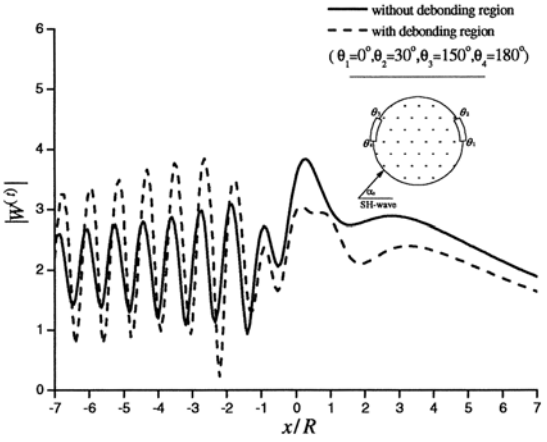

Fig. 12 The surface displacement amplitudes on the horizontal interface above an inclusion: $h/R = 1.5$, $\mu_2/\mu_1 = 3.23$, $\rho_2/\rho_1 = 1.52$, $\eta = 1.25$, $\alpha_0 = 0°$

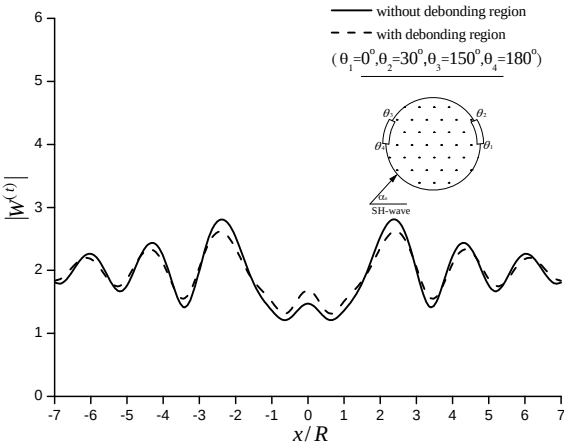

Fig. 15 The surface displacement amplitudes on the horizontal interface above an inclusion: $h/R = 1.5$, $\mu_2/\mu_1 = 3.23$, $\rho_2/\rho_1 = 1.52$, $\eta = 1.25$, $\alpha_0 = 90°$

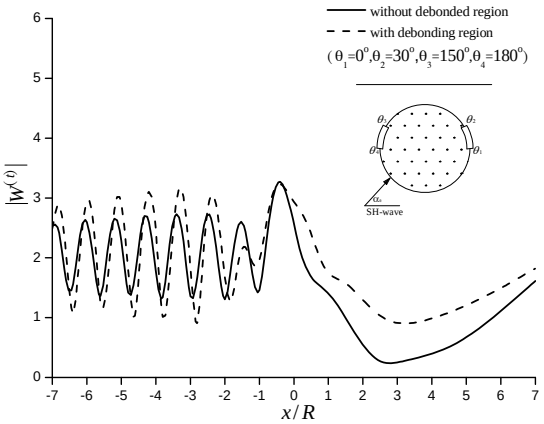

Fig. 13 The surface displacement amplitudes on the horizontal interface above an inclusion: $h/R = 1.5$, $\mu_2/\mu_1 = 3.23$, $\rho_2/\rho_1 = 1.52$, $\eta = 1.25$, $\alpha_0 = 30°$

release of much energy, in the region of $x/a > 0.0$, the displacement appears stable relatively with the value changing in the range of 2.0. However, with $\alpha_0 = 90°$, the whole wave energy could allocate averagely on the surface neighboring the inclusion, therefore, the displacement amplitudes linger around 2.0 in the two regions ($x/a < 0.0$ and $x/a > 0.0$).

The Figs. 12 to 15 display the surface displacement value in high frequency ($\eta = 1.25$). The angles of the debonding region are also: $\theta_1 = 0°$, $\theta_2 = 30°$, $\theta_3 = 150°$, $\theta_4 = 180°$. Relative to the low frequency state, the displacement gets larger and shaken. The surface displacement in the facing wave region ($x/a < 0.0$) appear vibrate seriously which shows an obvious dynamical feature. With the debonding region, the maximal value can get 3.82 around the area $x/a = 0.0$ with $\alpha_0 = 0°$, which is 27% larger than the value in low

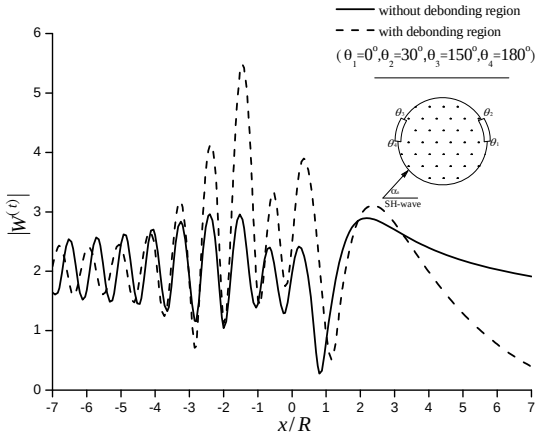

Fig. 16 The surface displacement amplitudes on the horizontal interface above an inclusion: $h/R = 1.5$, $\mu_2/\mu_1 = 0.38$, $\rho_2/\rho_1 = 0.77$, $\eta = 1.25$, $\alpha_0 = 0°$

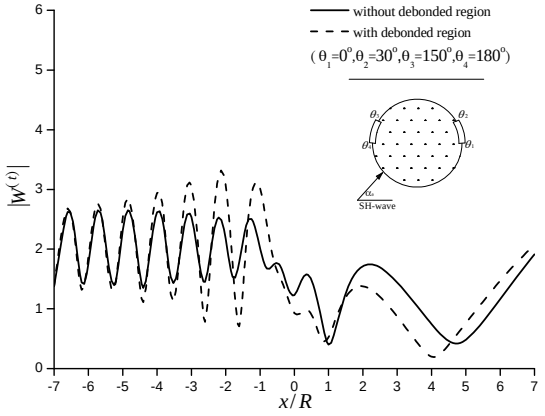

Fig. 17 The surface displacement amplitudes on the horizontal interface above an inclusion: $h/R = 1.5$, $\mu_2/\mu_1 = 0.38$, $\rho_2/\rho_1 = 0.77$, $\eta = 1.25$, $\alpha_0 = 30°$

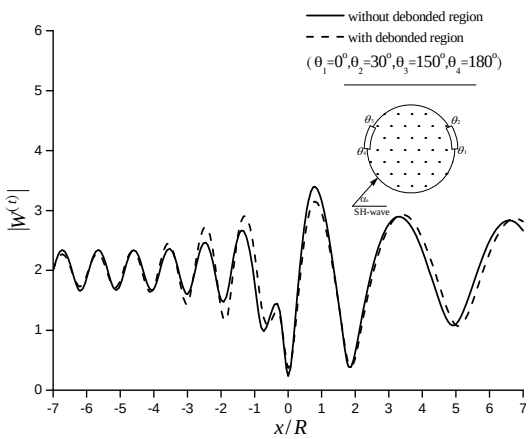

Fig. 18 The surface displacement amplitudes on the horizontal interface above an inclusion: $h/R = 1.5$, $\mu_2/\mu_1 = 0.38$, $\rho_2/\rho_1 = 0.77$, $\eta = 1.25$, $\alpha_0 = 60°$

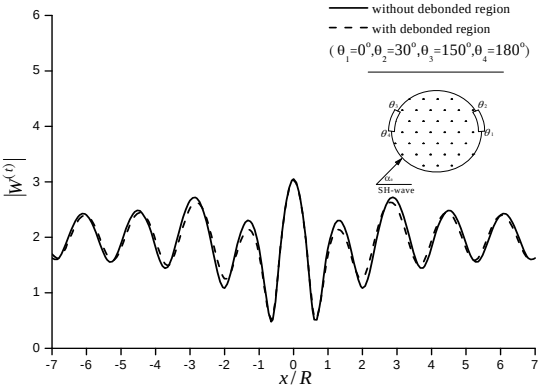

Fig. 19 The surface displacement amplitudes on the horizontal interface above an inclusion: $h/R = 1.5$, $\mu_2/\mu_1 = 0.38$, $\rho_2/\rho_1 = 0.77$, $\eta = 1.25$, $\alpha_0 = 90°$

frequency with the same incident angle. It is suggested that the wave might supply more energy to effect on the surface and promote the displacement in the facing region with high frequency. However, when the wave arrives at the back wave region ($x/a > 0.0$), the energy has released a large part and effects weaker on this region. Compared with the situation without the debonding region, in the high frequency, the numerical values with debonding region are distinctly larger than the ones without debonding region with low incident angle α_0. For instance, with $\alpha_0 = 0°$, the surface displacements in the facing region are nearly 20% ~ 30% larger than the values without debonding region, which suggesting that the debonding region participates the energy distribution and enhances the surface displacements in high frequency. Therefore, the influence by the debonding region in high frequency can not be neglected in the practical engineering.

As showed in Figs. 16 to 19, the displacement amplitudes with the concrete inclusion are listed in high frequency ($\eta = 1.25$). Compared with the situation of the steel inclusion, with the debonding region, the displacement value has a peak around the district $x/a = -2.0$ with the maximum 5.41 with $\alpha_0 = 0°$. It is implied that the softer inclusion such as the concrete inclusion might act more roughly than the harder one represented by the steel inclusion.

7. CONCLUSIONS

In this paper, the scattering of plane SH-wave from a partially debonded cylindrical elastic inclusion in half space is approached by complex function method and expansion method of wave function. However, we mainly focus on the ground motion by the debonding districts. But for the characteristic of the crack tips, such as the singularity and the concussive features, another approach is needed. From the above analysis, we can conclude that:

1. The frequency of the SH-wave takes an important part in the scattering problem in half space. With the low frequency, the surface displacement is less than the situation in high frequency. With the high frequency, the surface displacement could

appear shaken, this is an obvious dynamical feature.

2. The angle of the incident SH-wave α_0 has distinct effects on the surface displacement. With $\alpha_0 = 0°$, the value of the displacement could get the larger peak than the other incident angle. The key reason for this appearance is the energy distribution. Impacted by SH-wave tipsily, the main energy could gather on the facing wave region ($x/a < 0.0$) and result in the abrupt augment of the displacement. However, when the SH-wave attacks the medium vertically, the energy might distribute more averagely on the surface around the inclusion and the displacement value displays smaller.
3. The position of the debonding region has a significant influence to the surface displacement. When the debonding region is in the facing wave region, the surface displacement could be enlarged distinctly with low α_0. But, when the debonding region is stated in the back wave region ($x/a > 0.0$), the influence by the debonding region appears much smaller.
4. The characteristic of the inclusion is also concernful. Compared with the hard inclusion, the softer one such as the concrete inclusion might enlarge the surface displacement more easily.
5. In this paper, only the surface displacement impacted by the debonding region is researched. With regard to the dynamic stress intensity factor, it needs to be studied for another subject.

REFERENCES

1. Lee, V. W. and Trifunac, M. D., "Response of Tunnels to Incident SH-Waves," *ASCE, Engrg. Mechanics Div.*, 105, pp. 643–659 (1979).
2. Pao, Y. H. and Mow, C. C., "Diffraction of Elastic Waves and Dynamic Stress Concentrations," *New Work: Crane and Russak* (1973).
3. Lee, V. W., "On Deformations Near a Circular Underground Cavity Subjected to Incident Plane SH-Waves," *Proc. Application of Comp. Methods in Engry. Conf., Vol. II,Univ. of Southern California, Los Angeles, Calif.*, pp. 951–961 (1977).
4. Gregory, R. D., "An Expansion Theorem Applicable to Problems of Wave Propagation in an Elastic Half-Space," *Proc. Camb. Philos. Soc.*, 63, pp. 1341–1367 (1967).
5. Gregory, R. D., "The Propagation of Waves in an Elastic Half-Space Containing a Circular Cylindrical Cavity," *Proc. Camb. Philos. Soc.*, 67, pp. 689–710 (1967).
6. Datta, S. K., "Scattering of Elastic Waves," *Mechanics Today.*, 4, pp. 149–208 (1978).
7. Dravinski, M., "Ground Motion Amplification Due to Elastic Inclusions in a Half-Space," *International Journal Earthquake Engrg. and Struct. Dynamics.*, 11, pp. 313–335 (1983).
8. Manoogian, M. E. and Lee, V. W., "Diffraction of SH-Wave by Subsurface Inclusions of Arbitrary Shape," *ASCE, Eng. Mechanics Div.*, 122, pp. 123–129 (1996).
9. Lee, V. W., "Three-Dimensional Diffraction of Elastic Waves by a Spherical Cavity in an Elastic Half-Space. I: Closed-Form Solutions," *International Journal of Soil Dynamics and Earthquake Engrg.*, 7, pp. 149–161 (1988).
10. Chen, J. T., Chen, P. Y. and Chen, C. T., "Surface Motion of Multiple Alluvial Valleys for Incident Plane SH-Waves by Using a Semi-Analytical Approach," *Soil. Dyn. and Earthq. Eng.*, 28, pp. 58–72 (2008).
11. Chen, J. T., Chen, C. T., Chen, P. Y. and Chen, I. L., "A Semi-Analytical Approach for Radiation and Scattering Problems with Circular Boundaries," *Comput. Method. Appl. Mechanics and Eng.*, 196, pp. 2751–2764 (2007).
12. Belyaev, K. P., "Interaction of a Shear with an Elastic Cylindrical Inclusion Having a Crack Along its Contour," *Prikl. Mekh.*, 21, pp. 112–116 (1985).
13. Coussy, O., "Scattering of SH-Waves by a Cylindrical Inclusion Presenting an Interface Crack," *CR. Acad. Sci. Paris.*, 295, pp. 1043–1046 (1982).
14. Coussy, O., "Scattering of Elastic Waves by an Inclusion with an Interface Crack," *Wave Motion*, 6, pp. 223–236 (1983).
15. Yang, Y. and Norris, A. N., "Shear Wave Scattering from a Debonded Fiber," *Journal of Mechanics and Physics of Solids*, 39, pp. 273–294 (1991).
16. Norris, A. and Yang, Y., "Dynamic Stress on a Partially Bonded Fiber," *Journal of Applied Mechanics*, 58, pp. 404–409 (1991).
17. Yang, Y. and Norris, A., "Longitudinal Wave Scattering from a Partially Bonded Fiber," *Wave Motion*, 15, pp. 43–50 (1992).
18. Wang, Y. S. and Wang, D., "Scattering of Elastic Waves by a Rigid Cylindrical Inclusion Partially Debonded from its Surrounding Matrix, Part I. SH Case," *International Journal of Solids and Structures*, 33, pp. 2789–2815 (1996).
19. Wang, Y. S. and Wang, D., "Scattering of Elastic Waves by a Rigid Cylindrical Inclusion Partially Debonded from its Surrounding Matrix, Part II. P and SV Cases," *International Journal of Solids and Structures*, 33, pp. 2817–2840 (1996).
20. Wang, Y. S. and Wang, D., "Elastic Wave Scattering from a Partially Debonded Elastic Cylindrical Inclusion," *J Harbin Institute of Technology*, E-1, pp. 71–79 (1994).
21. Wang, Y. S. and Wang, D., "Diffraction of SH-Waves by a Circular Cavity with a Partially Debonded Liner," *Acta. Mechanics Sinica.*, 26, pp. 462–469 (1994).
22. Wang, Y. S., Yu, G. L. and Wang, D., "Dynamic Analysis of an Embedded Semicylindrical Foundation Partially Debonded from Soil," *Proc. of ICMSGE'94, China Translation and Printing Services Ltd.*, pp. 318–323 (1994).
23. Coussy, O., "Scattering of SH-Waves by a Rigid Elliptic Fiber Partially Debonded from its Surrounding Matrix," *Mechanics Res. Commu.*, 13, pp. 39–45 (1986).
24. Wang, Y. S., "Elliptic Arc Crack Subjected to Anti-

Plane Shear Wave," *Eng. Fract. Mechanics*, 48, pp. 289–297 (1994).

25. Wang, Y. S. and Wang, D., "Shear Wave Scattering from a Partially Debonded Elastic Elliptic Inclusion," *Mechanics, Res. Commu.*, 22, pp. 79–86 (1995).
26. Liu, D. K. and Wang, G. Q., "Antplane SH-Deformation of a Semi-Cylindrical Hill Above a Subsurface Cavity," *Acta. Mechanics Sinica.*, 3, pp. 209–218 (2006).
27. Liu, D. K. and Lin, H., "Scattering of SH-Waves by a Shallow Buried Cylindrical Cavity and the Ground Motion," *Explosion and Shock Waves*, 1, pp. 6–12 (2003).

(Manuscript received October 7, 2008,
accepted for publication April 23, 2009.)